Title

Active-site MMP-selective antibody inhibitors discovered from convex paratope synthetic libraries

Journal

Proceedings of the National Academy of Sciences of the United States of America, 113(52)

ISSN

0027-8424

Authors

Nam, Dong Hyun

Rodriguez, Carlos

Remacle, Albert G

et al.

Publication Date

2016-12-27

DOI

10.1073/pnas.1609375114

Peer reviewed

Active-site MMP-selective antibody inhibitors discovered from convex paratope synthetic libraries

Dong Hyun Nam[a], Carlos Rodriguez[a], Albert G. Remacle[b], Alex Y. Strongin[b], and Xin Ge[a,1]

[a]Department of Chemical and Environmental Engineering, University of California, Riverside, CA 92521; and [b]Inflammatory and Infectious Disease Center and Cancer Research Center, Sanford Burnham Prebys Medical Discovery Institute, La Jolla, CA 92037

Edited by K. Dane Wittrup, Adimab, LLC, Lebanon, NH, and accepted by Editorial Board Member David Baker November 21, 2016 (received for review June 9, 2016)

Proteases are frequent pharmacological targets, and their inhibitors are valuable drugs in multiple pathologies. The catalytic mechanism and the active-site fold, however, are largely conserved among the protease classes, making the development of the selective inhibitors exceedingly challenging. In our departure from the conventional strategies, we reviewed the structure of known camelid inhibitory antibodies, which block enzyme activities via their unusually long, convex-shaped paratopes. We synthesized the human Fab antibody library (over 1.25×10^9 individual variants) that carried the extended, 23- to 27-residue, complementarity-determining region (CDR)–H3 segments. As a proof of principle, we used the catalytic domain of matrix metalloproteinase-14 (MMP-14), a promalignant protease and a drug target in cancer, as bait. In our screens, we identified 20 binders, of which 14 performed as potent and selective inhibitors of MMP-14 rather than as broad-specificity antagonists. Specifically, Fab 3A2 bound to MMP-14 in the vicinity of the active pocket with a high 4.8 nM affinity and was similarly efficient (9.7 nM) in inhibiting the protease cleavage activity. We suggest that the convex paratope antibody libraries described here could be readily generalized to facilitate the design of the antibody inhibitors to many additional enzymes.

inhibitory antibody | long CDR | synthetic library | convex paratope | MMP

As key cellular proteinases, matrix metalloproteinase (MMP) family members control various physiological and pathological processes. Multiple diseases are associated with altered MMP expression and aberrant proteolysis, including cancer (1), wound healing (2), inflammatory diseases (3, 4), neurological pain (5, 6), and hypertension (7). There is consensus among researchers that the individual MMPs are promising drug targets in diversified pathologies and that inhibitor specificity is required for selective and successful MMP therapies (8–10).

However, achieving target specificity and selectivity in small-molecule MMP inhibitors is remarkably challenging (11, 12). Because the catalytic mechanism and catalytic domain fold are conserved among the MMP/ADAM (a disintegrin and metalloproteinase)/ADAMTS (ADAM with thrombospondin motifs) superfamily members, the available small-molecule inhibitors (most frequently, active-site zinc-chelating hydroxamates) target multiple proteinases, resulting in off-target side effects (8, 12–14). This aspect is problematic, given that some MMPs (e.g., MMP-14) are always protumorigenic, whereas some other MMPs are antitumorigenic in certain cancer microenvironments (15, 16). As a result, broad-spectrum hydroxamates failed in cancer clinical trials due to their low overall efficacy and side effects (13). Alternatively, antibody-based MMP inhibitors are emerging as both research tools and potential therapeutic agents (10, 17–21) because of (*i*) high affinity and specificity due to the large antigen–antibody interaction area and multiple complementarity-determining regions (CDRs), (*ii*) long half-life and well-defined action mechanisms, (*iii*) low immunogenicity and toxicity, and (*iv*) multiple MMPs potentially targetable by antibodies (9).

Natural protease inhibitors exhibit a convex-shaped conformation that inserts into the enzyme active site and blocks the substrate access and/or catalytic function (22). However, there is a low probability of generating antibodies with the convex antigen-binding sites (paratopes) from naive or immunized human or murine antibody libraries. The proteolytic pocket is often buried inside a major cleft or concave enzyme structure, and, as such, it is normally inaccessible by the cave-like, grooved, or flat antigen-binding surface in human and murine antibodies (23). In contrast, dromedary antibodies are enriched in the long CDR-H3s encoding the extended convex-shaped paratopes and, intriguingly, a large proportion of antibodies isolated from camels and llamas, compared with human and murine antibodies, bind the active-site pockets and inhibit enzymatic reactions (24–26). However, the camelid antibodies would evoke an immune response in humans, and the availability of these animals is limited.

With the hypothesis that convex paratopes are inhibitory, we designed human Fab libraries in which the long, convex-shaped, camelid-like paratopes were incorporated into the human antibody scaffold (27) (Fig. S1). In our current proof-of-principle study, we screened these libraries for the inhibitors of MMP-14, a proinvasive and prometastatic human proteinase (28, 29). As a result of our screens, we isolated a panel of selective Fabs with a high inhibitory potency against MMP-14. We are now confident that these libraries and similar libraries that exhibit the long, convex paratopes will be a valuable source of the inhibitory antibodies capable of targeting multiple additional enzymes, the active pockets of which are not readily accessible by the conventional human antibodies.

Results

Design and Construction of Long CDR-H3 Synthetic Fab Libraries. A large proportion of camelid heavy-chain antibodies (V_HHs) exhibit enzyme-inhibiting functions (24, 25). Structure studies suggest that

Significance

The matrix metalloproteinase (MMP) family members are promising drug targets in diversified pathologies. Clinical trial failures taught us that selective, rather than broad-specificity, inhibitors are required for successful MMP therapies. Achieving target selectivity with small-molecule MMP inhibitors, however, is exceedingly difficult. Because the antigen-binding sites in conventional antibodies are predominantly incompatible with the concave reaction pockets of MMPs, design of inhibitory antibodies, an attractive alternative for selective inhibition, is also challenging. We synthesized human antibody libraries encoding extended convex antigen-binding sites and isolated a panel of inhibitory Fabs that selectively and efficiently inhibited MMP-14, a promising drug target in cancer. The pipeline we established can now be readily applied for the generation of inhibitory antibodies targeting multiple additional enzymes besides MMPs alone.

Author contributions: D.H.N. and X.G. designed research; D.H.N., C.R., and A.G.R. performed research; D.H.N., A.G.R., A.Y.S., and X.G. analyzed data; and D.H.N., A.G.R., A.Y.S., and X.G. wrote the paper.

The authors declare no conflict of interest.

This article is a PNAS Direct Submission. K.D.W. is a Guest Editor invited by the Editorial Board.

[1]To whom correspondence should be addressed. Email: xge@engr.ucr.edu.

This article contains supporting information online at www.pnas.org/lookup/suppl/doi:10.1073/pnas.1609375114/-/DCSupplemental.

inhibition is mediated by the extended CDR-H3s coding for the convex-shaped paratopes that penetrate into the enzyme catalytic cleft (23, 26). Consistent with the studies by others (30), our in-depth analysis of over 950 individual camelid antibodies available from the international ImMunoGeneTics (IMGT), Kabat, and abYsis databases determined that there is a bimodal distribution in their CDR-H3 length with peaks at 12 and 19 residues (Fig. S2*A*). It is likely that these long CDR-H3s compensate for a lack of light chains (V_Ls). A similar analysis of over 90,000 human and murine antibody sequences revealed that the length of their CDR-H3s is characterized by a single peak Gaussian distribution at 12 and nine residues, respectively. In addition, our analysis suggests that relative to murine/human CDR-H3s, camelid CDR-H3 regions are enriched in Cys, positively charged (Arg and Lys), and hydrophilic (Gly, Ser, Thr, and Asn) residues, whereas the level of hydrophobic residues (Phe, Val, and Ile) is decreased. These amino acid preferences likely contribute to the additional disulfide bonds in camelid antibodies and, in general, to the integrity and improved solubility of the CDR-H3 loops (31, 32).

To mimic amino acid use in the camelid repertoire, a degenerate codon XYZ containing different proportions of the nucleotides at each of the three codon positions was custom-designed for insertion into a human heavy-chain (V_H) framework (Fig. S2*B*). Oligonucleotides encoding the 23-, 25-, and 27-residue-long CDR-H3s (significantly longer than in humans) were synthesized (Fig. S3, step 1) and assembled using mesophilic T4 DNA polymerase and T4 DNA ligase without amplification to achieve high fidelity and low bias (33) (Fig. S3, step 2). To remove the truncated and reading frame-shifted fragments, the assembled CDR-H3 constructs were subjected to full-length selection by their cloning into the N-terminal sequence of β-lactamase (34) (Fig. S3, step 3). The diversities of the selected CDR-H3-23, CDR-H3-25, and CDR-H3-27 were 2.1×10^8, 0.85×10^8, and 0.80×10^8, respectively. DNA sequencing verified that 98% of clones (129 of 131 clones) were functional. Selected CDR-H3s were then incorporated into a synthetic Fab phage library (35) to generate 1.25×10^9 Fab clones (4.6×10^8, 3.4×10^8, and 4.5×10^8 for CDR-H3-23, CDR-H3-25, and CDR-H3-27, respectively; Fig. S3, step 4). The V_Ls have fixed sequences in CDR-L1/CDR-L2 and a 3- to 7-aa length variability in CDR-L3. Sequencing of the constructs indicated that 91% of Fab clones (92 of 101 clones) exhibited the full-length CDR-H3s with 23, 25, or 27 residues, and that the diversity in the other CDRs, such as CDR-L3, CDR-H1, and CDR-H2 was still preserved well in the single V_H/V_L framework. In addition, 87% of randomly picked clones (34 of 39 clones) were able to produce detectable levels of the Fab-pIII fusions suitable for phage panning.

Isolation of Anti–MMP-14 Inhibitory Antibodies. After three rounds of panning with elution steps that used the N-terminal inhibitory domain of tissue inhibitor of metalloproteinase-2 (n-TIMP-2), monoclonal ELISA of 288 randomly picked clones isolated 126 positive Fab clones from which 77 were sequenced, resulting in the identification of 20 unique Fabs carrying the long CDR-H3 regions (Table 1). These CDR-H3 regions were enriched in basic (Arg and Lys) and hydrophilic (Asn, Gln, Thr, and Ser) residues, although the levels of negatively charged (Asp and Glu) and hydrophobic (Ala, Ile, Val, Phe, and Trp) residues were decreased (Fig. S4), likely leading to better solubility of Fabs and more efficient interactions with the negatively charged surface of the MMP-14 active-site cavity (22). The CDR-H3 loops of 3D9 and 3A6 constructs exhibited two Cys residues each and were potentially able to form intraloop disulfide bonds. The V_L sequencing results showed >95% amino acid sequence identity, supporting the dominant roles of V_Hs for binding and inhibition.

Table 1. Isolated MMP-14 binding Fabs from synthetic antibody libraries of long and normal CDR-H3 designs

Library (size)	Clone*	CDR-H3 sequence (length)	Binding affinity	Inhibition potency†	Selectivity‡
Long CDR-H3 (1.25×10^9)	3A2	VKLQKDKSHQWIRNLVATPYGRYVMDY (27)	3.8 nM	9.7 nM	Exclusive
	3E2	GIKGLVFTGSQMKMLRRGNYNWYVMDY (27)	47 nM	42 nM	Exclusive
	3D9	RLMAYHGSCSSRLCQTAISPQRYAMDY (27)	6.4 nM	61 nM	Exclusive
	2B5	IGVNAWAVKMSQRMLATRGSGWYVMDY (27)	24 nM	240 nM	Exclusive
	3G9	ATNEKFRRKSLQVRLLMRSWLAYAMDY (27)	160 nM	390 nM	16.7
	33D2	SKYGPASRQLASRTSWSGPRGKYGMDY (27)	120 nM	420 nM	9.6
	3F3	LYNGWLMVEGIGSAREGPTWYAMDY (25)	34 nM	970 nM	n.d.
	33F3	GVRGNKLRLLSSRSGLMESHYVMDY (25)	1.0 μM	2.3 μM	n.d.
	33D4	SVHMKLSNKILSGWSWNNSFYAMDY (25)	460 nM	3.9 μM	n.d.
	32D1	MSLHRNFNQQGRSRLLGRMPRTYGMDY (27)	350 nM	4.2 μM	n.d.
	3A6	RPCKACRTRLELVRRGMDSGLRYGMDY (27)	980 nM	4.2 μM	n.d.
	33C4	PTTSRVNKKLFRVSVLHPGSYGMDY (25)	220 nM	4.6 μM	n.d.
	3E9	NGRYPGFLKRAHKRLLNFKAYVMDY (25)	51 nM	6.0 μM	n.d.
	32C2	SQHAKKSTIIRMLEHQSRSGMQYVMDY (27)	150 nM	8.0 μM	n.d.
	32E10	LDRDRYIHVGRAGNTYSNYYYVMDY (25)	9.7 nM	Noninhibitory	n.d.
	32C11	EIHMLSRQARYLRDGRRPRGSMYVMDY (27)	29 nM	Noninhibitory	n.d.
	2H9	GTSFQVRCVLYRLLSPGRYVMDY (23)	120 nM	Noninhibitory	n.d.
	3B2	STAATTLSRMSRSYWTIQLPYGMDY (25)	590 nM	Noninhibitory	n.d.
	2E4	SARLRLRGNHDRRRSKSVYYRPYVMDY (27)	840 nM	Noninhibitory	n.d.
	33F5	NFRVESAGRPGKTVLRKDGKYAMDY (25)	1.6 μM	Noninhibitory	n.d.
Normal (3×10^{10})	S2H2	GVWYSSAMDY (10)	2.5 nM	noninhibitory	n.d.
	S3G2	YGYSAYWYALDY (12)	2.6 nM	noninhibitory	n.d.
	S3B5	GYSSYGYALDY (11)	2.7 nM	noninhibitory	n.d.
	S33E8	YSHPFWSAMDY (11)	3.7 nM	noninhibitory	n.d.
	S32A1	FFYGSSSWYYSGAMDY (16)	3.9 nM	noninhibitory	n.d.
	S32A9	SHGYYSGLDY (10)	9.1 nM	noninhibitory	n.d.

n.d., not determined.

*Clones are ranked based on inhibition potency (or binding affinity for noninhibitory clones).

†Determined by FRET assays. "Noninhibitory" indicates no signs of inhibition when Fab was used at 2–4 μM.

‡Only Fabs with an inhibition potency of $IC_{50} < 500$ nM were measured. Exclusive selectivity indicated background ELISA signals with MMP-2/MMP-9 at 500 nM Fabs. Folds of selectivity were determined by the ratio of Fab concentrations, which gave the same ELISA signals, between MMP-2/MMP-9 and MMP-14.

The 20 selected Fabs were produced in *Escherichia coli* periplasmic space with a typical yield of the purified proteins of 0.5–2 mg/L medium (Fig. S5*A*). Size exclusion chromatography confirmed that the isolated Fab samples were highly soluble and present as monomers in solution, without detectable aggregation (Fig. S5*B*). After storage at 4 °C for 1 mo, purified Fab samples were still stable without visible aggregates or degradation as determined by SDS/PAGE (Fig. S5*C*).

The binding affinity of the purified Fabs with MMP-14 was measured using ELISA. The binding EC_{50} value of the samples was in a 3.8 to 1,600 nM range (Table 1). The most efficient binders included 3A2 (3.8 nM), 3D9 (6.4 nM), and 32E10 (9.7 nM), and the EC_{50} values of the additional five Fabs were between 24 and 51 nM (Fig. 1*A*, Table 1, and Fig. S6). Fourteen (70%) of the 20 Fabs we purified inhibited MMP-14 proteolysis of the fluorescent peptide substrate (7-methoxycoumarin-4-yl)Acetyl-Lys-Pro-Leu-Gly-Leu-(3-[2,4-dinitrophenyl]-L-2,3-diaminopropionyl)-Ala-Arg-NH_2, with IC_{50} values between 9.7 nM and 8 μM (Table 1). The presence of 70% of the inhibitory clones among the binders is remarkably high, especially if compared with previous studies of the inhibitory antibodies (hit rates of 2.5% and 17%) (17, 36). The inhibition IC_{50} values of Fabs 3A2, 3E2, and 3D9 were 9.7 nM, 42 nM, and 61 nM, respectively, and the IC_{50} values of three additional Fabs were in 240–420 nM range (Fig. 1*A* and Table 1). Fab 3E9, the most enriched clone we isolated through phage panning (22 repeated sequences), showed a moderate, 51 nM binding capacity, but its inhibitory potency was low (IC_{50} = 6.0 μM) (Table 1 and Fig. S6*A*). The enrichment of this clone was likely a result of a high growth rate and/or high expression level relative to other Fab clones. Similarly, a few high-affinity Fabs [e.g., 32E10 (EC_{50} = 9.7 nM)] did not inhibit MMP-14, suggesting that efficient binding does not directly correlate with high inhibitory potency of the antibody (Fig. S6*B*). To test whether the most promising inhibitory Fabs are resistant to MMP-14 proteolysis (37), Fabs 3A2, 3E2, 3D9, and 2B5 were incubated with MMP-14 (at an enzyme/antibody molar ratio of 1:5 or 1:10) at pH 7.5 and 37 °C for 1 or 16 h. No significant degradation of the antibodies was observed under these conditions (Fig. S7).

In a control experiment, in the course of phage panning, we used a highly diversified antibody library (3×10^{10} variants) exhibiting the normal 1- to 17-residue CDR-H3s (35) and phage elution steps with n-TIMP-2. This experiment resulted in six individual Fabs bound to MMP-14 with a low nanomolar affinity; however, none was inhibitory even at 2–4 μM (Table 1). These findings strongly support the expectation that the convex-shaped paratopes formed by the long CDR-H3 segments play an essential role in generating the inhibitory antibodies.

Because selectivity is the prime parameter for the MMP inhibitors, we next assessed if the most promising Fabs would cross-react with other MMPs. According to the ELISA results, all of the six Fabs we tested were highly selective for MMP-14. Indeed, Fabs 3A2, 3E2, 3D9, and 2B5 were incapable of binding to MMP-2 or MMP-9 even at a high concentration of 500 nM. The two other Fabs, 33D2 and 3G9, were ∼10- to 20-fold more selective for MMP-14 relative to MMP-2 and MMP-9 (Fig. 1*B*).

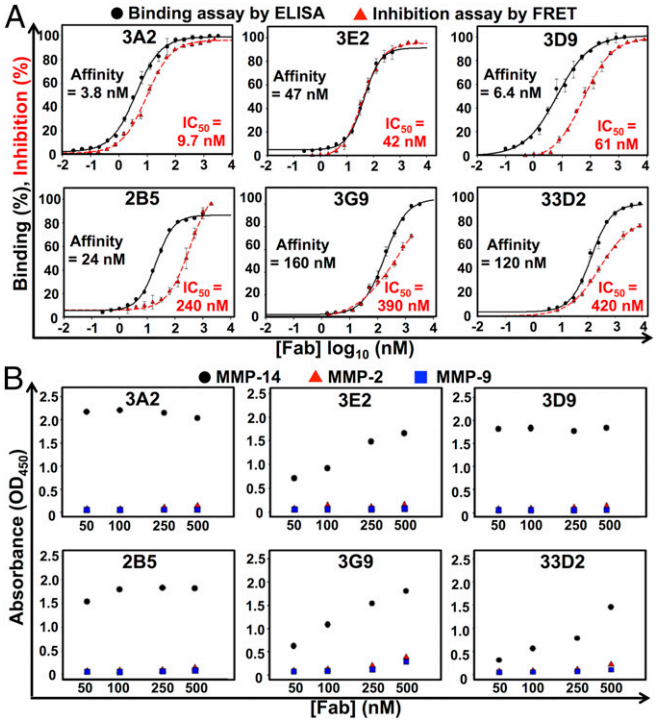

Fig. 1. Biochemical characterizations of representative high-potency inhibitory Fabs. (*A*) Dose–response curves of binding affinity (black) and IC_{50} (red) values of purified Fabs. Quenched-fluorescent substrate peptide (1 μM) and 1 nM catalytic domain MMP-14 (1 nM) were used in FRET inhibition assays. Error bars represent the SD of triplicate experiments. (*B*) Binding selectivity toward MMP-14 (black circles) over MMP-2 (red triangles) and MMP-9 (blue squares) tested by ELISA.

Fab 3A2 Is a Highly Potent Competitive Selective Inhibitor of MMP-14. The most efficient inhibitor, Fab 3A2, was studied in a more detail to determine both its inhibitory mechanism and its binding mode. The binding kinetics of Fab 3A2 to MMP-14 were examined using surface plasmon resonance spectroscopy (Fig. 2*A*). A concentration-dependent saturable binding of 10–20 nM Fab 3A2 to immobilized MMP-14 was observed. Apparent equilibrium binding constants were determined with an average kinetic association coefficient (k_{on}) equal to 3.68×10^5 $M^{-1}{\cdot}s^{-1}$ and an average kinetic dissociation coefficient (k_{off}) of $1.79 \times 10^{-3}s^{-1}$. The equilibrium dissociation constant (K_d) calculated from the k_{off}/k_{on} ratio was 4.85 nM, and this value agreed well with the ELISA data (Fig. 1*A*).

The IC_{50} value of Fab 3A2 was 9.7 ± 1.2 nM and similar to the IC_{50} value of n-TIMP-2 (IC_{50} = 5.1 ± 2.4 nM) and GM6001, a potent, albeit nonselective, hydroxamate inhibitor of MMPs (IC_{50} = 2.1 ± 0.6 nM) (Fig. 2*B*). At 500 nM, Fab 3A2 completely inhibited MMP-14 (98%), but not MMP-2 or MMP-9 (0.2% and 2.5% inhibition, respectively) (Fig. 2*C*). At the similar conditions, n-TIMP-2 and GM6001 inhibited MMP-2/MMP-9/MMP-14 nonselectively (83–100% inhibition), confirming that they are broad-spectrum inhibitors of the MMP family (38, 39).

Competitive ELISA results (Fig. 2*D*) indicated that increasing concentrations of n-TIMP-2 reduced the binding of Fab 3A2 to MMP-14, likely suggesting an overlap of their respective binding sites in MMP-14. To determine the type of inhibition, a series of kinetic assays in the presence of 0, 250, and 500 nM Fab 3A2 was performed. The obtained Lineweaver–Burk plots demonstrated an unchanged maximum velocity (V_{max}) and an elevated Michaelis constant (K_m) when the Fab concentration increased, indicating that Fab 3A2 performed as a competitive inhibitor of MMP-14 proteolytic activity (Fig. 2*E*).

To identify the binding site of Fab 3A2, we performed Ala scanning mutagenesis of MMP-14. Eight residue positions (T190, F198, Y203, F204, N229, N231, S251, and F260) were selected for Ala substitution, based on the following criteria: (*i*) distinct in MMP-14 relative to MMP-2 and MMP-9 (Fig. S8*A*), (*ii*) within a distance of 15 Å from the catalytic Zn^{2+}, (*iii*) exhibiting an exposed respective side chain, and (*iv*) near the S1′ subsite (40, 41). The resulting MMP-14 mutants were expressed in the periplasmic space of *E. coli* (42). Compared with wild-type MMP-14, these MMP-14 mutants exhibited reduced, albeit still substantial, specific activity (0.4–6.6% relative to the wild type), which was used as the basis for our inhibition measurements (Fig. S8*B*). ELISA and

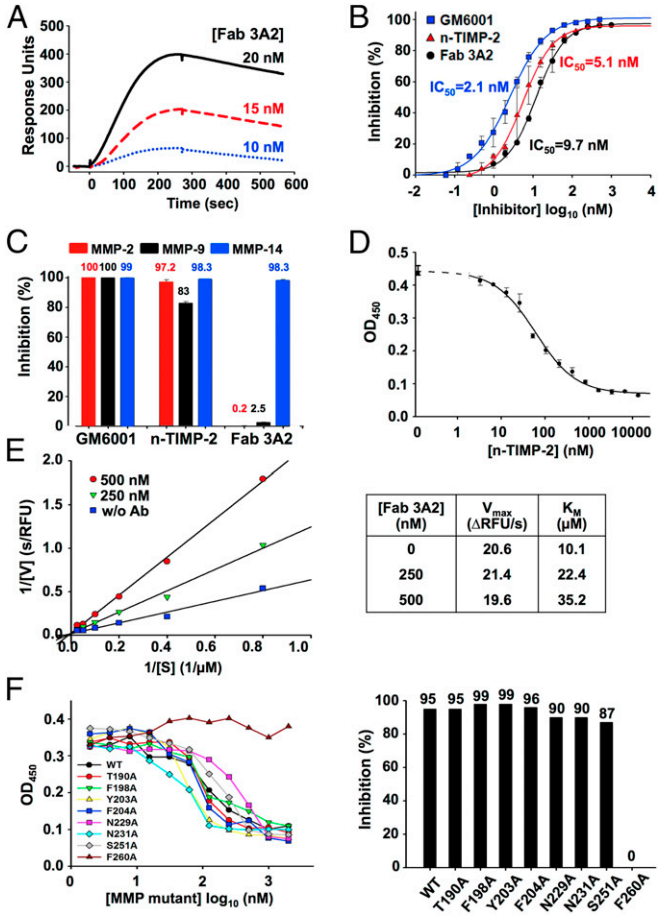

Fig. 2. Binding affinity and inhibition potency measurements, inhibitor type determination, and epitope mapping of Fab 3A2. (*A*) Binding kinetics of 10 nM (blue dotted line), 15 nM (red dashed line), and 20 nM (black solid line) Fab 3A2 to catalytic domain MMP-14 (cdMMP-14) measured by surface plasmon resonance. On average, $k_{on} = 3.68 \times 10^5$ ($M^{-1} \cdot S^{-1}$), $k_{off} = 1.79 \times 10^{-3}$ (s^{-1}), and $K_d =$ 4.85 nM. (*B*) Fab 3A2 inhibited cdMMP-14 proteolytic activity on the peptide substrate with a potency of 9.7 ± 1.2 nM, the same order of magnitude as n-TIMP-2 (5.1 ± 2.4 nM) and GM6001 (2.1 ± 0.6 nM). (*C*) Inhibition selectivity tests of Fab 3A2, GM6001, and n-TIMP-2 toward MMP-2/MMP-9/MMP-14. In contrast to GM6001 and n-TIMP-2, Fab 3A2 showed selectivity to MMP-14 and did not inhibit MMP-2/MMP-9. (*D*) Competitive ELISA of Fab 3A2 with n-TIMP-2. Serially diluted n-TIMP-2 samples were incubated with 10 nM Fab 3A2 in streptavidin wells coated with biotinylated cdMMP-14. The signals were generated by anti-Fab–HRP. (*E*, *Left*) Lineweaver–Burk plots of MMP-14 with 0, 250, and 500 nM Fab 3A2. RFU, relative fluorescent units. (*E*, *Right*) Calculated V_{max} and K_m are shown. (*F*) Epitope determination by competitive ELISA and inhibition assays. Eight MMP-14 single-site mutants were prepared by periplasmic expression without refolding. Fab 3A2 (10 nM) was incubated with increasing amounts of MMP-14 mutant on a surface coated with wild-type MMP-14. An inhibition assay was performed using 50 nM MMP-14 mutant, 5 μM Fab 3A2, and 1 μM quenched fluorescent substrate.

inhibition assay results showed that the performance of all these mutants, except F260A, did not differ significantly from the performance of the original MMP-14 (Fig. S8*C*). In contrast, the F260A MMP-14 mutant lost its ability to bind to the Fab 3A2 and, consistently, the catalytic activity of this mutant was resistant to inhibition by Fab 3A2 (Fig. 2*F*). Our results, especially when combined, imply that Fab 3A2 is a competitive selective inhibitor of MMP-14, that the binding site of this antibody overlaps with the binding site of TIMP-2, and that the extended CDR-H3 loop of Fab 3A2 likely accesses the F260 residue from the S1′ subsite in the MMP-14 active-site pocket.

Fab 3A2 Inhibits MMP-14 Collagenolysis and Activation of the MMP-2 Proenzyme. Activation of the MMP-2 proenzyme is the most well-known function of cell-surface MMP-14 (43). To evaluate the effect of the Fab 3A2 on MMP-2 activation, we used human fibrosarcoma HT1080 cells, which produce high levels of MMP-2 naturally. To stimulate activation of the MMP-2 proenzyme by cellular MMP-14, the cells were treated with tetradecanoyl phorbol acetate, and then coincubated with Fab 3A2 or 3E9 [a weak inhibitory Fab (IC_{50} = 6 μM) as a negative control] or with GM6001 (a highly potent hydroxamate MMP inhibitor as a positive control). The status of MMP-2 was next analyzed by gelatin zymography (Fig. 3*A*). As expected, 10 μM GM6001 (used at a high concentration due to its low stability in aqueous solutions of cellular assays) totally repressed MMP-2 activation. Although >40% of proMMP-2 was processed when no Fab or Fab 3E9 was applied, 200 nM Fab 3A2 inhibited 82% of MMP-14–dependent MMP-2 activation in HT1080 cells. These results were consistent with the peptide inhibition assays, confirming that Fab 3A2 inhibited MMP-14 with a high potency in HT1080 cells.

Because MMP-14 is a collagenase, we then tested if Fab 3A2 affected MMP-14 collagenolysis. For these purposes, we used human mammary epithelial 184B5 cells stably transfected with MMP-14 (44). As a control, we used the original 184B5 cells, which naturally produce a low level of MMP-14. Cells were plated on a layer of type I collagen with or without the inhibitors. Following incubation for 5 d, cells were gently detached and the collagen layer was fixed and then stained using Coomassie Blue R-250 stain to visualize the degraded, unstained areas. Fig. 3*B* shows that collagen was almost completely degraded (<10% of collagen remained) by 184B5–MMP14 cells. As expected, GM6001, at a high concentration of 25 μM, blocked 96% of collagenolysis. Similarly, Fab 3A2, at a low concentration of 250 nM, repressed 93% of collagenolysis in 184B5–MMP14 cells. These data suggest that Fab 3A2 performs as a potent inhibitor of MMP-14 in cell-based assays and represses MMP-14 proteolysis of its natural, physiologically relevant substrates.

Discussion

Monoclonal antibodies (mAbs) are ubiquitous in biomedical research and medicine. A variety of methodologies have been developed for recombinant antibody discovery. The design of mAbs with selective proteinase-inhibiting functions, however, remains a significant challenge because of (*i*) the low antigenicity of the catalytic centers that are normally buried in the enzyme globule and (*ii*) the lack of reliable function-based selection methods. For example, in an attempt to isolate the antibodies capable of inhibiting serpase (a membrane-associated serine protease encoded by the fibroblast activation protein gene), 40 efficiently binding single-chain variable fragment (scFv) clones were identified from a human naive scFv phage display library of over 1×10^{10} variants, but only a single scFv construct exhibited inhibition function with a micromolar range potency (36).

The inhibitor/binder ratio was significantly improved when a specific selection procedure was added to phage panning (17). Thus, the use of TIMP-2, a natural protein inhibitor of MMP-14, as a competitive eluent of the antigen-binding clones from the MMP-14 bait led to the discovery of 12 inhibitory constructs from 70 affinity clones (17% hit rate). In addition, TIMP-2 binds to the native MMP-14 enzyme rather than to the misfolded and denatured species of the proteinase. As a result, the use of TIMP-2 allows one to disregard the antibodies that bind to the denatured MMP-14 species.

Extending these findings, our current methodology combined this epitope-specific elution with a synthetic antibody library design. Our approach resulted in the identification of 14 inhibitory antibodies from the 20 isolated MMP-14 binders [i.e., with a high (70%) hit rate]. The rationale of our antibody repertoire design was based on sequence analysis of the inhibitory camelid V_HHs

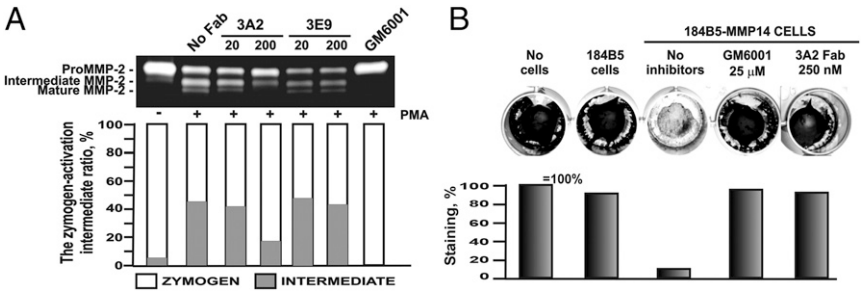

Fig. 3. Inhibition function of Fab 3A2 on MMP-14 proteolytic activities toward physiological substrates. (*A*) Gelatin zymography of MMP-14–dependent activation of proMMP-2. (*B*) Fab 3A2 inhibition on degradation of type I collagen mediated by cellular MMP-14. The intensity of the bands and collagen was quantified using the digitized images and ImageJ (NIH) software. In gelatin zymography, a proenzyme/activation intermediate ratio was expressed as the percentage of the proenzyme and the intermediate, each relative to their total amount.

and the crystal structures of the multiple V_HH/enzyme complexes. These analyses revealed that the extended CDR-H3s provided the enlarged antigen-binding surface and convex paratopes that penetrated into the catalytic cleft and inhibited the enzymatic reaction (22, 24). In addition to the camelid single-domain antibodies, inhibitory antibodies were recently developed using antibody scaffolding of the cow. In the latter, the protruding domains encoded by the ultralong, up to 60-residue, CDR-H3s are frequent (45, 46). In agreement, structural studies of the inhibitory antibodies isolated from human naive libraries also suggested that insertion of the long CDR-H3 variable loops (up to 19 residues) into the substrate-binding pocket is required to achieve efficient inhibition of membrane type serine protease 1 (matriptase) (37, 47). Although the alternative inhibitory mechanisms are also well known, including those mechanisms that inactivate enzymes by inducing conformational changes or by blocking substrate access (48, 49), multiple inhibitory antibodies exhibit unusually long CDR-H3s, implying that the extended CDR-H3s are vital for enzyme inhibition. Therefore, in this proof-of-concept study, 23- to 27-residue-long CDR-H3s were arbitrarily designed and synthesized presumably to form convex-shaped paratopes. The presence of these long CDR-H3s is infrequent in the natural human IgGs (50). Our results clearly suggest that the constructed long CDR-H3s (but not the normal-length CDR-H3s) are inhibitory when MMP-14 was used as bait (Table 1). However, the optimal CDR-H3 length for inhibiting certain enzymes probably needs to be adjusted according to the targets (i.e., the topology of reaction pockets).

Our current study resulted in 14 inhibitory antibodies of which Fab 3A2, without any maturation, was highly potent against MMP-14. The inhibitory potency of this Fab was similar to the inhibitory potency of n-TIMP-2, the natural inhibitor of MMPs, and GM6001, one of the most effective, albeit broad-specificity, hydroxamate MMP inhibitors. However, in contrast to n-TIMP-2 or GM6001, Fab 3A2 was highly selective and did not exhibit off-target effects with other MMP family members, such as MMP-2/MMP-9. Importantly, Fab 3A2 efficiently repressed the activity of cellular MMP-14 on its physiological substrates, including MMP-2 and type I collagen. In addition to Fab 3A2, our research led to the discovery of five other potent inhibitors with promising selectivity against MMP-14, with an IC_{50} value less than 500 nM. Based on the relationship between binding affinity and inhibition potency, the 14 inhibitory Fabs isolated in this study can be grouped into four clusters (Fig. S9): group 1, the seven clones with high binding affinity and high inhibition potency, having the potential to serve as leads suitable for further characterizations; group 2, two clones with high binding affinity and low inhibition potency, presumably which paratopes partially contribute to inhibition; and groups 3 and 4, five clones with moderate or low binding affinity and moderate inhibition potency, probably binding to inhibitory epitopes with suboptimal strengths. Overall, this inhibitory Fab panel provides a rich pool of lead candidates for the further selection of therapeutics and fine-tuning of pharmacological properties through affinity maturation and solubility/stability improvement.

Mutagenesis of MMP-14, rather than a linear peptide approach (51), followed by the expression of mutants in the periplasm of *E. coli* (42), allowed us to map the Fab 3A2 epitope roughly in the MMP-14 catalytic domain. Our data indicate that Fab 3A2 targets the S1′ pocket of MMP-14 and directly competes with both substrate and n-TIMP-2 binding (Fig. 4*A*). Approximately 22% of the Fab 3A2 CDR-H3 residues are positively charged (Lys/Arg/His), suggesting potential interactions between the CDR-H3 loop and the negatively charged active-site vicinity of MMP-14 (Fig. 4*B*).

The MMP family members are promising drug targets in pathologies ranging from atherosclerosis and stroke to cancer and arthritis. The long CDR-H3 synthetic Fab libraries we constructed have already been applied for the identification of inhibitory antibodies to other MMPs, including MMP-2 and MMP-9. It is highly likely that the general methodology we developed and successfully used in our study could be readily reused to design the selective antibody inhibitors to additional individual MMPs. These selective inhibitors can also be exploited as research tools to shed more light on MMP functionality in normal and pathophysiological conditions. Furthermore, our antibody design technology could be generalized and applied to other targets outside of the MMP family. Overall, our proof-of-principle study suggests that the synthetic antibody

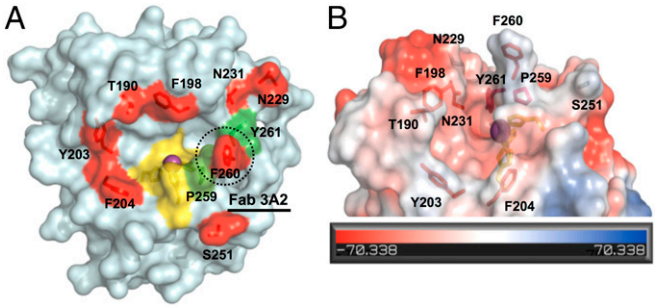

Fig. 4. Inhibition mechanisms by structure interpretation. (*A*) Top view of the cdMMP-14 reaction site. Three His residues (yellow) of the catalytic motif (HEXXHXXGXXH) coordinate the catalytic zinc (purple). P259, F260, and Y261 (green) form the specific S1′ cleft. Eight mutation sites for epitope mapping are shown in red. Competitive ELISA and inhibition assays (Fig. 2*F*) suggested that Fab 3A2 bound at F260 (black dotted circle). (*B*) Side view of MMP-14 reaction cleft and vicinity as an electrostatic surface model. Protruding F260 is responsible for the formation of a relatively deep S1′ cleft with the catalytic zinc (purple) at the bottom of the cleft. The concave active site is predominantly negatively charged. Images were generated using PyMOL based on the MMP-14 crystal structure (Protein Data Bank 1BQQ).

libraries with the extended CDR-H3 segments have a potential to generate selective function-blocking antibodies to multiple enzymes in which druggable pockets are buried deeply inside the protein globule and which cannot be accessed by the antibodies designed by current methodologies.

Methods

Degenerate polynucleotides encoding the randomized 23-, 25-, and 27-residue-long CDR-H3 segments were chemically synthesized. To mimic the camelid antibody CDR-H3 repertories, customized XYZ codons were designed (Fig. S2*B*). The long CDR-H3 fragments were assembled by overlap extension without PCR amplification (33). Functional full-length CDR-H3 fragments were selected and cloned into phagemids to generate synthetic human Fab libraries. The constructed phage libraries were subjected to three rounds of panning against the immobilized catalytic domain of MMP-14. The isolated Fab clones were biochemically characterized by ELISA, FRET assays, and epitope mapping. Inhibitory function in the cellular context was also tested. Detailed experimental procedures are provided in *SI Methods*.

ACKNOWLEDGMENTS. This work was supported by the National Science Foundation Faculty Early Career Development Program 1453645 (to X.G.), NIH Grant R01 GM115672 (to X.G.), and California Breast Cancer Research Program Developmental and Exploratory Award 21IB-0104 (to X.G. and A.Y.S.).

1. Overall CM, Kleifeld O (2006) Tumour microenvironment - opinion: Validating matrix metalloproteinases as drug targets and anti-targets for cancer therapy. *Nat Rev Cancer* 6(3):227–239.
2. Liu Y, et al. (2009) Increased matrix metalloproteinase-9 predicts poor wound healing in diabetic foot ulcers. *Diabetes Care* 32(1):117–119.
3. Hu J, Van den Steen PE, Sang QX, Opdenakker G (2007) Matrix metalloproteinase inhibitors as therapy for inflammatory and vascular diseases. *Nat Rev Drug Discov* 6(6):480–498.
4. Elkington PTG, O'Kane CM, Friedland JS (2005) The paradox of matrix metalloproteinases in infectious disease. *Clin Exp Immunol* 142(1):12–20.
5. Kawasaki Y, et al. (2008) Distinct roles of matrix metalloproteases in the early- and late-phase development of neuropathic pain. *Nat Med* 14(3):331–336.
6. Dev R, Srivastava PK, Iyer JP, Dastidar SG, Ray A (2010) Therapeutic potential of matrix metalloprotease inhibitors in neuropathic pain. *Expert Opin Investig Drugs* 19(4):455–468.
7. Castro MM, Tanus-Santos JE (2013) Inhibition of matrix metalloproteinases (MMPs) as a potential strategy to ameliorate hypertension-induced cardiovascular alterations. *Curr Drug Targets* 14(3):335–343.
8. Deu E, Verdoes M, Bogyo M (2012) New approaches for dissecting protease functions to improve probe development and drug discovery. *Nat Struct Mol Biol* 19(1):9–16.
9. Drag M, Salvesen GS (2010) Emerging principles in protease-based drug discovery. *Nat Rev Drug Discov* 9(9):690–701.
10. Botkjaer KA, et al. (2016) Development of a specific affinity-matured exosite inhibitor to MT1-MMP that efficiently inhibits tumor cell invasion in vitro and metastasis in vivo. *Oncotarget* 7(13):16773–16792.
11. Overall CM, López-Otín C (2002) Strategies for MMP inhibition in cancer: Innovations for the post-trial era. *Nat Rev Cancer* 2(9):657–672.
12. Cathcart J, Pulkoski-Gross A, Cao J (2015) Targeting matrix metalloproteinases in cancer: Bringing new life to old ideas. *Genes Dis* 2(1):26–34.
13. Turk B (2006) Targeting proteases: Successes, failures and future prospects. *Nat Rev Drug Discov* 5(9):785–799.
14. Zucker S, Cao J (2009) Selective matrix metalloproteinase (MMP) inhibitors in cancer therapy: Ready for prime time? *Cancer Biol Ther* 8(24):2371–2373.
15. Gialeli C, Theocharis AD, Karamanos NK (2011) Roles of matrix metalloproteinases in cancer progression and their pharmacological targeting. *FEBS J* 278(1):16–27.
16. Decock J, Thirkettle S, Wagstaff L, Edwards DR (2011) Matrix metalloproteinases: Protective roles in cancer. *J Cell Mol Med* 15(6):1254–1265.
17. Devy L, et al. (2009) Selective inhibition of matrix metalloproteinase-14 blocks tumor growth, invasion, and angiogenesis. *Cancer Res* 69(4):1517–1526.
18. Sela-Passwell N, et al. (2011) Antibodies targeting the catalytic zinc complex of activated matrix metalloproteinases show therapeutic potential. *Nat Med* 18(1):143–147.
19. Naito S, et al. (2012) Development of a neutralizing antibody specific for the active form of matrix metalloproteinase-13. *Biochemistry* 51(44):8877–8884.
20. Sandborn WJ, et al. (2016) Randomised clinical trial: A phase 1, dose-ranging study of the anti-matrix metalloproteinase-9 monoclonal antibody GS-5745 versus placebo for ulcerative colitis. *Aliment Pharmacol Ther* 44(2):157–169.
21. Ager EI, et al. (2015) Blockade of MMP14 activity in murine breast carcinomas: implications for macrophages, vessels, and radiotherapy. *J Natl Cancer Inst* 107(4):djv017.
22. Fernandez-Catalan C, et al. (1998) Crystal structure of the complex formed by the membrane type 1-matrix metalloproteinase with the tissue inhibitor of metalloproteinases-2, the soluble progelatinase A receptor. *EMBO J* 17(17):5238–5248.
23. Lauwereys M, et al. (1998) Potent enzyme inhibitors derived from dromedary heavy-chain antibodies. *EMBO J* 17(13):3512–3520.
24. De Genst E, et al. (2006) Molecular basis for the preferential cleft recognition by dromedary heavy-chain antibodies. *Proc Natl Acad Sci USA* 103(12):4586–4591.
25. Desmyter A, et al. (1996) Crystal structure of a camel single-domain V-H antibody fragment in complex with lysozyme. *Nat Struct Biol* 3(9):803–811.
26. Schmitz KR, Bagchi A, Roovers RC, van Bergen en Henegouwen PM, Ferguson KM (2013) Structural evaluation of EGFR inhibition mechanisms for nanobodies/VHH domains. *Structure* 21(7):1214–1224.
27. Hoogenboom HR (2005) Selecting and screening recombinant antibody libraries. *Nat Biotechnol* 23(9):1105–1116.
28. Genís L, Gálvez BG, Gonzalo P, Arroyo AG (2006) MT1-MMP: Universal or particular player in angiogenesis? *Cancer Metastasis Rev* 25(1):77–86.
29. Morrison CJ, Butler GS, Rodríguez D, Overall CM (2009) Matrix metalloproteinase proteomics: Substrates, targets, and therapy. *Curr Opin Cell Biol* 21(5):645–653.
30. Griffin LM, et al. (2014) Analysis of heavy and light chain sequences of conventional camelid antibodies from Camelus dromedarius and Camelus bactrianus species. *J Immunol Methods* 405:35–46.
31. Nguyen VK, Hamers R, Wyns L, Muyldermans S (2000) Camel heavy-chain antibodies: diverse germline V(H)H and specific mechanisms enlarge the antigen-binding repertoire. *EMBO J* 19(5):921–930.
32. De Genst E, Saerens D, Muyldermans S, Conrath K (2006) Antibody repertoire development in camelids. *Dev Comp Immunol* 30(1-2):187–198.
33. Ge X, Mazor Y, Hunicke-Smith SP, Ellington AD, Georgiou G (2010) Rapid construction and characterization of synthetic antibody libraries without DNA amplification. *Biotechnol Bioeng* 106(3):347–357.
34. Seehaus T, Breitling F, Dübel S, Klewinghaus I, Little M (1992) A vector for the removal of deletion mutants from antibody libraries. *Gene* 114(2):235–237.
35. Persson H, et al. (2013) CDR-H3 diversity is not required for antigen recognition by synthetic antibodies. *J Mol Biol* 425(4):803–811.
36. Zhang J, et al. (2013) Identification of inhibitory scFv antibodies targeting fibroblast activation protein utilizing phage display functional screens. *FASEB J* 27(2):581–589.
37. Farady CJ, Sun J, Darragh MR, Miller SM, Craik CS (2007) The mechanism of inhibition of antibody-based inhibitors of membrane-type serine protease 1 (MT-SP1). *J Mol Biol* 369(4):1041–1051.
38. Butler GS, et al. (1999) The specificity of TIMP-2 for matrix metalloproteinases can be modified by single amino acid mutations. *J Biol Chem* 274(29):20391–20396.
39. Vandenbroucke RE, Libert C (2014) Is there new hope for therapeutic matrix metalloproteinase inhibition? *Nat Rev Drug Discov* 13(12):904–927.
40. Nagase H (2001) Substrate specificity of MMPs. *Matrix Metalloproteinase Inhibitors in Cancer Therapy*, eds Clendeninn NJ, Appelt K (Humana Press, Totowa, NJ), pp 403–420.
41. Gupta SP, Patil VM (2012) Specificity of binding with matrix metalloproteinases. *Matrix Metalloproteinase Inhibitors*, ed Gupta SP (Springer, Basel), pp 35–56.
42. Nam DH, Ge X (2016) Direct production of functional matrix metalloproteinase–14 without refolding or activation and its application for in vitro inhibition assays. *Biotechnol Bioeng* 113(4):717–723.
43. Strongin AY, et al. (1995) Mechanism of cell surface activation of 72-kDa type IV collagenase. Isolation of the activated form of the membrane metalloprotease. *J Biol Chem* 270(10):5331–5338.
44. Golubkov VS, et al. (2006) Membrane type-1 matrix metalloproteinase confers aneuploidy and tumorigenicity on mammary epithelial cells. *Cancer Res* 66(21):10460–10465.
45. Liu T, et al. (2015) Rational design of antibody protease inhibitors. *J Am Chem Soc* 137(12):4042–4045.
46. Zhang Y, et al. (2013) Functional antibody CDR3 fusion proteins with enhanced pharmacological properties. *Angew Chem Int Ed Engl* 52(32):8295–8298.
47. Schneider EL, et al. (2012) A reverse binding motif that contributes to specific protease inhibition by antibodies. *J Mol Biol* 415(4):699–715.
48. Wu Y, et al. (2007) Structural insight into distinct mechanisms of protease inhibition by antibodies. *Proc Natl Acad Sci USA* 104(50):19784–19789.
49. Ganesan R, et al. (2009) Unraveling the allosteric mechanism of serine protease inhibition by an antibody. *Structure* 17(12):1614–1624.
50. Wu TT, Johnson G, Kabat EA (1993) Length distribution of CDRH3 in antibodies. *Proteins* 16(1):1–7.
51. Shiryaev SA, et al. (2013) A monoclonal antibody interferes with TIMP-2 binding and incapacitates the MMP-2-activating function of multifunctional, pro-tumorigenic MMP-14/MT1-MMP. *Oncogenesis* 2:e80.
52. Nam DH, Ge X (2013) Development of a periplasmic FRET screening method for protease inhibitory antibodies. *Biotechnol Bioeng* 110(11):2856–2864.
53. Pardon E, et al. (2014) A general protocol for the generation of nanobodies for structural biology. *Nat Protoc* 9(3):674–693.
54. Fellouse FA, Sidhu SS (2013) Making antibodies in bacteria. *Making and Using Antibodies*, ed Kase MR (CRC Press, Boca Raton, FL), pp 151–172.
55. Knight CG, Willenbrock F, Murphy G (1992) A novel coumarin-labelled peptide for sensitive continuous assays of the matrix metalloproteinases. *FEBS Lett* 296(3):263–266.
56. Dunbar J, et al. (2016) SAbPred: A structure-based antibody prediction server. *Nucleic Acids Res* 44(W1):W474–W478.

Supporting Information

Nam et al. 10.1073/pnas.1609375114

SI Methods

Construction of Long CDR-H3 Fab Phage Libraries. Six degenerate polynucleotides encoding the randomized 23-, 25-, and 27-residue-long CDR-H3 segments and the partial framework region 3 (FR3) and FR4 were synthesized by IDT. To mimic the camelid antibody CDR-H3 repertories, customized XYZ codons were synthesized using the following proportion of nucleotides: X = 38% G, 19% A, 26% T, and 17% C; Y = 31% G, 34% A, 17% T, and 18% C; and Z = 24% G and 76% C. The XYZ codons were used to construct the 23-residue-long CDR-H3 fragments. The standard NNS codons were used for constructing the 25- and 27-residue-long CDR-H3s. The long CDR-H3 fragments were assembled by overlap extension without PCR amplification using T4 DNA polymerase and T4 DNA ligase (33). The assembled long CDR-H3 fragments were gel-purified, digested with AflII/HindIII, and cloned into the N terminus of the β-lactamase gene. CDR-H3 libraries were transformed into *Escherichia coli* Jude-I (DH10B harboring the F′ factor derived from XL1-Blue) and incubated on 2× YT agar plates supplemented with 0.5 mM isopropyl β-D-1-thiogalactopyranoside and 50 μg/mL ampicillin to remove stop codons and reading frame shifts (34). Selected in-frame long CDR-H3 fragments were cloned into AflII/BsmBI sites on phagemids of a synthetic Fab antibody library (35). The constructed Fab phage libraries carrying long CDR-H3s were transformed into *E. coli* XL1-Blue by electroporation, and library quality was validated by DNA sequencing. The expression profile of 39 randomly picked Fab phage clones was tested by Western blotting using anti-Fab–horseradish peroxidase (HRP) conjugates.

Production and Biotinylation of MMP-2, MMP-9, MMP-14, and n-TIMP-2. The catalytic domains of MMP-2 and MMP-14 were cloned, expressed, purified, and refolded as described previously (52). The catalytic domain of MMP-9 was produced without refolding by soluble expression in the periplasmic space of *E. coli* (42). Enzymatic activities of MMPs were analyzed by cleavage assays using a quenched fluorescent peptide substrate Mca-Lys-Pro-Leu-Gly-Leu-Dap(Dnp)-Ala-Arg-NH_2 (Bachem). The reactions were performed in Tris-buffered saline [TBS; 50 mM Tris·HCl (pH 7.5), 150 mM NaCl, 5 mM $CaCl_2$, 100 μM $ZnCl_2$] in the presence of 1–40 μM substrate and 10 nM MMP. Fluorescent signals (relative fluorescent units) with the excitation at 328 nm and the emission at 393 nm were monitored continuously at 10-s intervals using a Synergy H4 microplate reader (BioTek) to determine the K_m and k_{cat}. The purified MMP-2, MMP-9, and MMP-14 catalytic domains were biotinylated using EZ-Link Sulfo-NHS-LC-Biotin reagent (Pierce) and applied in phage panning and ELISA. MMP-14 mutant genes were constructed by overlapping PCR and similarly expressed and isolated from the periplasm of *E. coli*. The n-TIMP-2 was produced by *E. coli* periplasmic expression and affinity-purified as described in a previous study (42).

Phage Panning and Monoclonal ELISA. Standard protocols were applied for phage preparations and ELISA, with modifications (53, 54). Briefly, ~10^{13} phage particles of the constructed long CDR Fab library were depleted by incubation in wells of a microtiter plate coated with streptavidin at ambient temperature for 1 h. The streptavidin-depleted phage library was then transferred to wells of a microtiter plate coated with streptavidin, followed by biotinylated MMP-14. Incubation was continued at ambient temperature for 1 h. After washing 10 times with TBS containing 0.1% Tween 20 (TBST) and five times with TBS, MMP-14 binders were eluted by incubation with 6 μM n-TIMP-2 at ambient temperature for 1 h. The remaining phages were further eluted with 100 mM triethylamine. In the second and third rounds of selection, to increase stringency, the wells were washed 20 times with TBST, followed by five times with TBS. The antigen concentration was reduced to twofold in the third round. Monoclonal phage ELISA was performed in wells of a microtiter plate coated with streptavidin in 0.5% gelatin, followed by biotinylated MMP-14. The wells coated with biotinylated BSA, but not with MMP-14, were used as a control. The coated plates were incubated with the supernatant aliquots of the monoclonal phage cultures. Anti-M13–HRP conjugate and 3,3′,5,5′-tetramethylbenzidine (TMB) were added to the wells. The reaction was stopped by acidification using sulfuric acid. The absorbance was measured at 450 nm. The clones with signal ratios of MMP-14 to BSA over 5 were considered positive.

Cloning, Expression, and Purification of Fabs. Selected Fab genes were cloned into the Fab expression vector containing the PhoA promoter, a STII leader peptide, and a His tag at the C terminus of the V_H (54). After expression in *E. coli* BL21 at 30 °C overnight, Fabs were purified from the periplasmic fraction by nickel-nitrilotriacetic acid chromatography, dialyzed against 50 mM Hepes and 150 mM NaCl (pH 6.8), and analyzed by SDS/PAGE. The concentrations of Fabs were measured with a NanoDrop 2000 instrument (Thermo Scientific).

Fab ELISA. Purified Fab was serially diluted in MMP-14–coated wells, followed by incubation at ambient temperature for 1 h. Bound Fabs were detected using the anti-Fab–HRP conjugate. The EC_{50} was calculated from a four-parameter, logistic, curve-fitting analysis. In the competitive ELISA for epitope mapping, 10 nM Fab 3A2 was incubated with 0–2,000 nM MMP-14 mutants for 2 h and transferred to the streptavidin-coated wells with biotinylated wild-type MMP-14 for 15 min. Bound Fab 3A2 was detected using the anti-Fab–HRP conjugate.

MMP Inhibition Assay. The enzymatic activity of the wild-type and mutant MMP-14 in the presence of inhibitory Fabs was measured at 37 °C by monitoring the hydrolysis of the fluorogenic peptide with the excitation at 328 nm and the emission at 393 nm (55). Typically, 0–8,000 nM Fab was incubated with 1 nM MMP-14 in TBS buffer for 1 h at ambient temperature, and the reaction was then initiated by adding the substrate to a final concentration of 1 μM. Fluorescence was recorded continuously for 30 min, and the initial reaction rates and inhibition constants were calculated by fitting the data to Eq. **S1**, where V_i is the initial velocity in the presence of inhibitor, V_o is the initial velocity in the absence of inhibitor, and $[I]$ is the inhibitor concentration:

$$\frac{V_i}{V_o}\% = \frac{1}{1+\frac{[I]}{IC_{50}}} \times 100. \qquad \textbf{[S1]}$$

To determine the type of inhibition, the initial velocity of MMP-14 was measured as a function of substrate concentration (0–40 μM) at several fixed concentrations of Fab (0–500 nM). The values of apparent K_m and V_{max} were derived by linearization according to the Lineweaver–Burk equation.

Surface Plasmon Resonance Analysis Using Biacore. MMP-14 was immobilized on a CM5 sensor chip via amine coupling. Fab samples (5–20 nM each) were injected over the surface for the binding experiments performed at 25 °C. The data were processed using a monophasic model for nonlinear curve fitting with possible

mass transport considered. The rate constants k_{on} and k_{off} were calculated using the BIAevaluation version 4.1 package (Pharmacia).

Gelatin Zymography. Fibrosarcoma HT1080 cells, which expressed MMP-14 on the cell surface, were stimulated for 24 h in serum-free DMEM supplemented with 50 ng/mL tetradecanoyl phorbol acetate (Sigma–Aldrich) alone or in the presence of the indicated 20–200 nM concentration of Fabs. The status of MMP-2 in the conditioned medium aliquots was analyzed using a precast 10% (wt/vol) acrylamide gel copolymerized with 0.1% gelatin (Life Technologies). After electrophoresis, the gel was incubated twice for 30 min at ambient temperature in 2.5% (wt/vol) Triton X-100 and then for 16–18 h at 37 °C in 50 mM Tris·HCl (pH 7.4) containing 10 mM $CaCl_2$, 1 μM $ZnCl_2$, and 0.02% NaN_3. The gel was then stained with Coomassie Blue R-250 to visualize the bands with gelatinolytic activity. The broad-spectrum hydroxamate MMP inhibitor GM6001 (10 μM) was added to the cells and used as a positive control to inhibit MMP-14 catalytic activity.

MMP-14–Mediated Degradation of Type I Collagen. Twenty-four-well plates were coated with neutralized, chilled rat tail type I collagen (300 μg/mL, 350 μL in PBS) for 3 h at 37 °C and air-dried for 16 h. The collagen coating was washed with water and rehydrated for 2 h at 37 °C in 500 μL of serum-free DMEM. The human mammary epithelial 184B5 cells, which did not produce MMP-14, served as a negative control. The 184B5-MMP14 cells were obtained by transfecting 184B5 cells with the full-length MMP-14 gene (44). Cells (5×10^4) in DMEM/2% (vol/vol) FBS were seeded onto the collagen-coated wells and allowed to attach for 3 h. The medium was then removed and replaced with 350 μL of serum-free DMEM alone or DMEM containing 250 nM Fab or 50 μM GM6001. The cells were incubated for 5 d. On day 3, the medium was replaced with fresh serum-free DMEM alone or containing the molecules of interest. On day 5, cells were detached with 2 mM EDTA, and the collagen was then fixed with 4% (wt/vol) paraformaldehyde and stained with Coomassie Blue R-250.

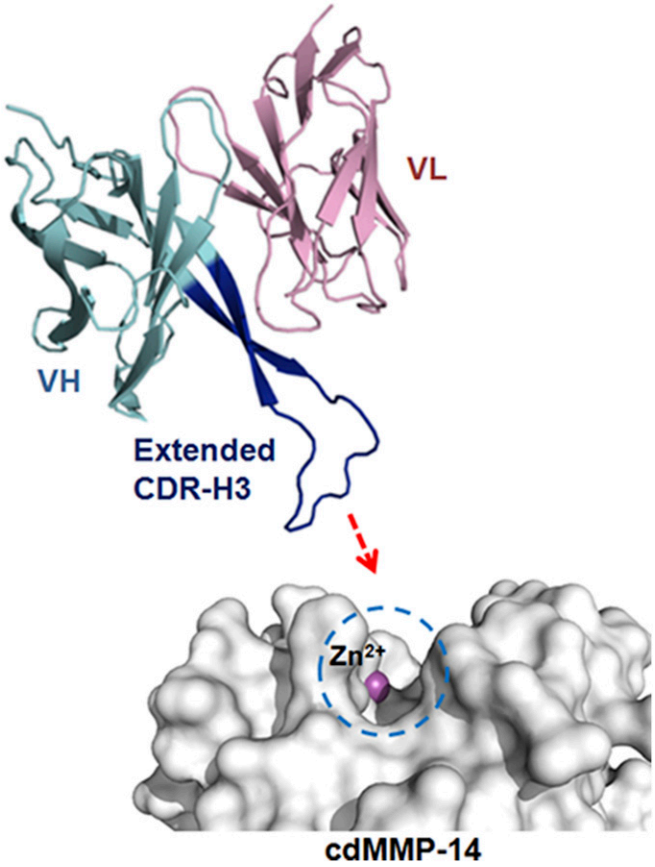

Fig. S1. Scheme shows that a convex antibody paratope formed by an extended CDR-H3 mediates enzyme inhibition. The active site of the MMP-14 catalytic domain (cdMMP-14; gray) has a concave structure, with the catalytic Zn^{2+} at the bottom of the pocket (magenta). Fab 3A2 (V_H, cyan; V_L, pink) binds to the cdMMP-14 reaction pocket through its long 27-residue CDR-H3 loop (blue). A model of Fab 3A2 was generated using the antibody structure prediction server SAbPred (56), based on the 3A2 CDR-H3 sequence (Table 1). Images were generated using PyMOL.

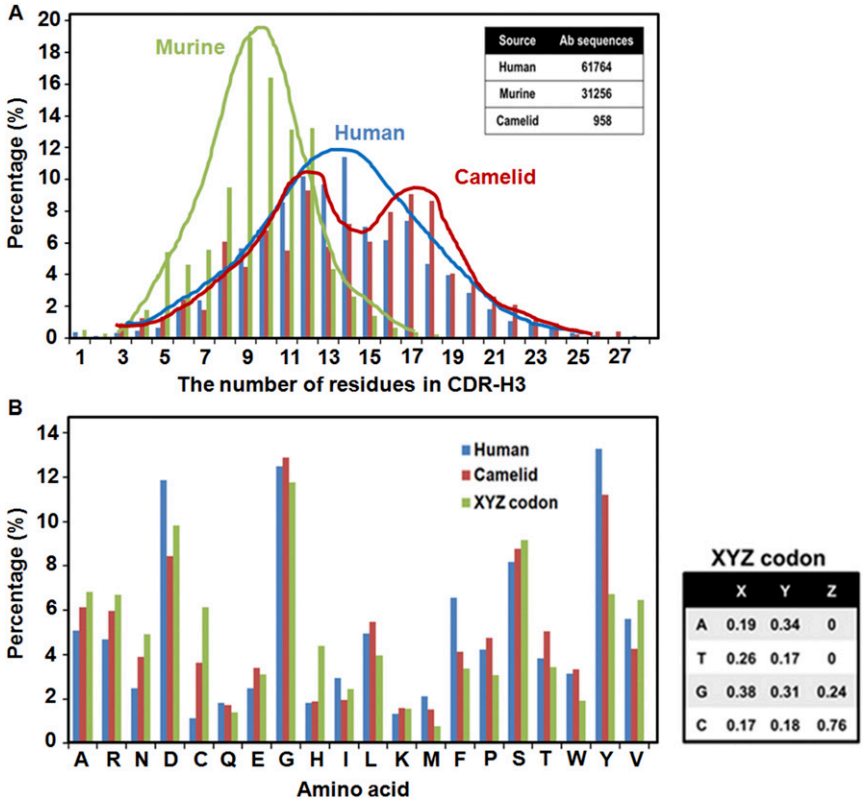

Fig. S2. Human, murine, and camelid antibody repertoire analysis. (*A*) CDR-H3 length distributions. The CDR-H3 length of camelid antibodies shows a bimodal distribution, distinctly different from Gaussian distribution of human and murine antibodies with averages at 12 and nine residues, respectively. The sequences of antibodies were obtained from the IMGT (international ImMunoGeneTics), Kabat, and abYsis antibody databases, with the numbers of available sequences used for statistics indicated in the inserted table. (*B*) Amino acid compositions of human and camelid CDR-H3s and a customized degenerate codon called XYZ. Camelid antibodies carry more Cys, less hydrophobic residues (Phe, Val, and Ile), more positively charged residues (Arg and Lys), and more hydrophilic residues (Gly, Ser, Thr, and Asn). To mimic these features, a degenerate codon XYZ was custom-designed to bias the diversity toward the amino acid use in camelid CDR-H3 sequences. The inserted table indicates nucleotide proportions of XYZ at each of the three codon positions.

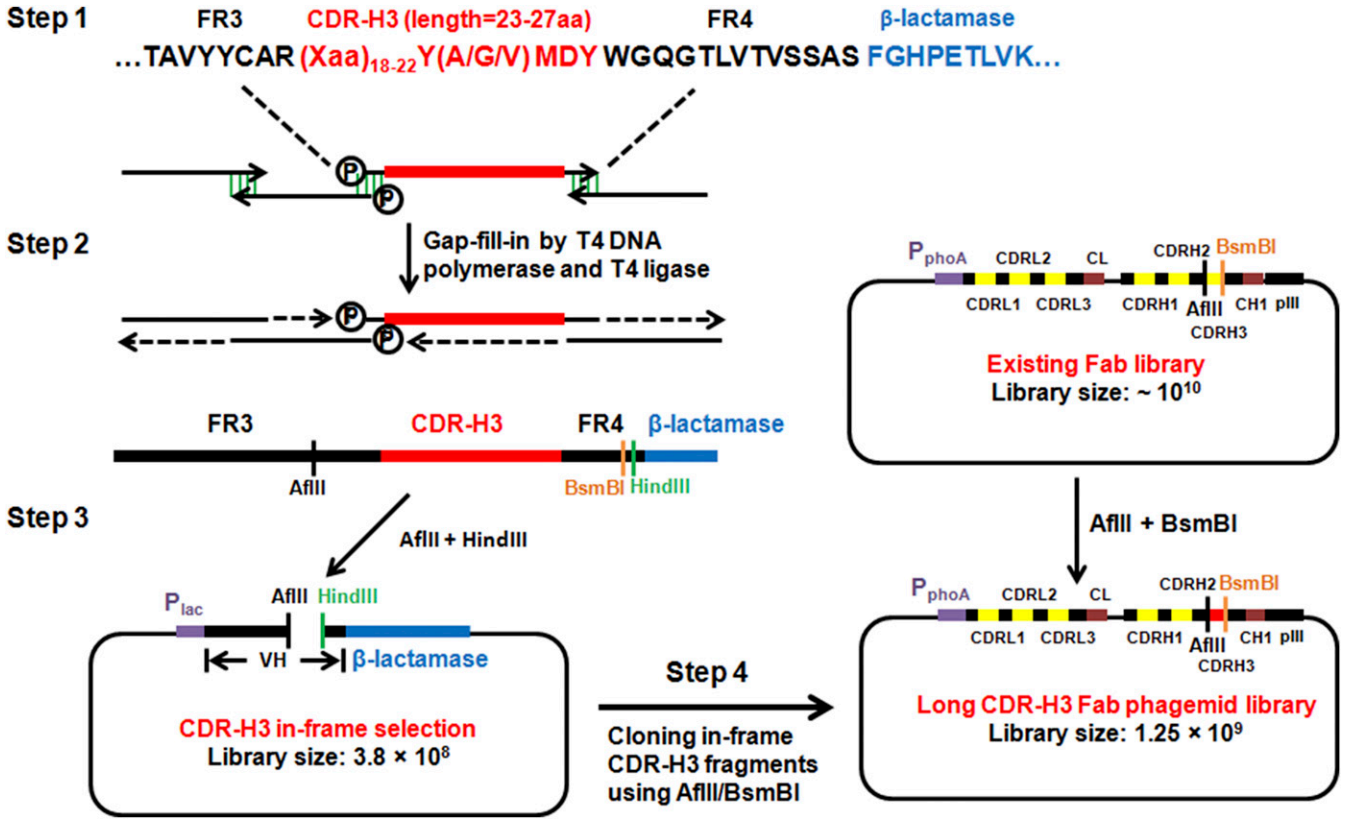

Fig. S3. Construction of synthetic antibody libraries with long CDR-H3s. (Step 1) Hybridization of degenerate oligonucleotides encoding long CDR-H3s with 23, 25, and 27 aa. (Step 2) CDR-H3 fragment assembly by T4 DNA polymerase and T4 DNA ligase. (Step 3) Assembled long CDR-H3 genes were subjected for full-length in-frame selection by fusing with β-lactamase. CDR-H3s (3.8×10^8) were generated after in-frame selection. (Step 4) Cloning of the in-frame CDR-H3s into an existing Fab library to construct a synthetic antibody library carrying long CDR-H3s with 23, 25, and 27 aa. The final library diversity was 1.25×10^9.

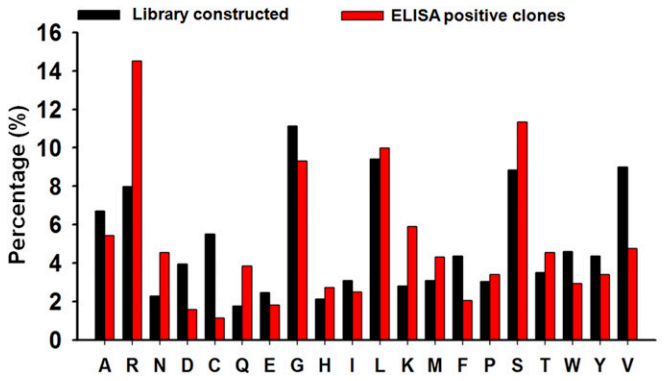

Fig. S4. CDR-H3 amino acid frequency in the constructed library (100 clones) and selected ELISA-positive Fabs (77 clones).

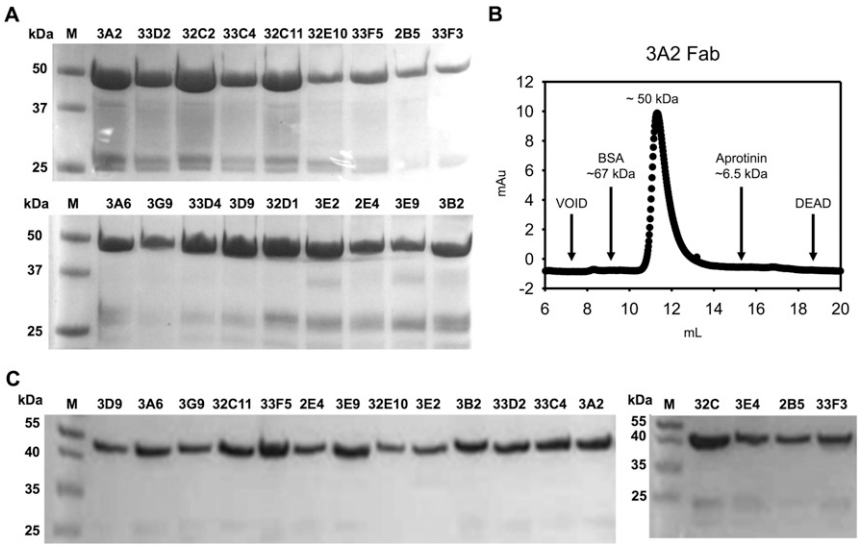

Fig. S5. Purity and storage stability of produced Fabs and size exclusion chromatography (SEC) analysis of Fab 3A2. (*A*) Nonreducing SDS/PAGE of purified long CDR-H3 Fabs. Typical yields of Fabs were 0.5–2 mg/L in *E. coli* after purification. Trace amounts (typically <2%) of unassembled V_HS are presented at ~27 kDa. (*B*) SEC of purified Fab 3A2 using an analytical Superdex 75 10/300 GL column (GE Health). Fab 3A2 was eluted as a monomer, without any detectable level of aggregates. (*C*) Nonreducing SDS/PAGE of purified Fabs after storage for 1 mo at 4 °C.

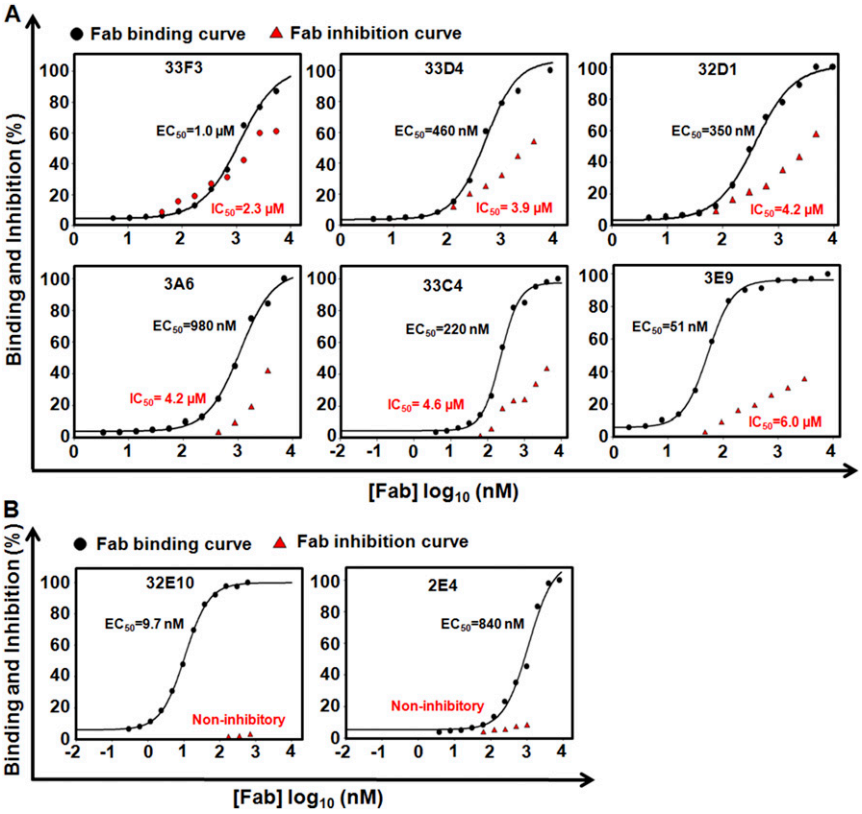

Fig. S6. Dose–response curves of EC_{50} (black) and IC_{50} (red) values of representative low-potency inhibitory Fabs (*A*) and noninhibitory Fabs (*B*). Quenched-fluorescent substrate peptide (1 μM) and cdMMP-14 (1 nM) were used in FRET inhibition assays.

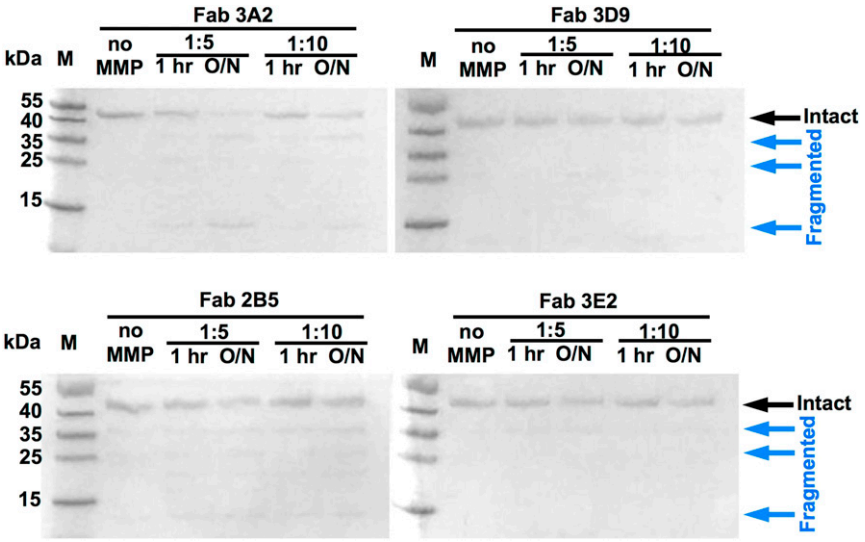

Fig. S7. Stability of purified Fabs in the presence of MMP-14 at an enzyme/Fab ratio of 1:5 or 1:10. Mixtures at pH 7.5 were incubated at 37 °C for 1 h or overnight (O/N; 16 h). Except for the Fab 3A2 overnight sample at the 1:5 ratio, none of the other tested conditions resulted in significant cleavage of Fabs by MMP-14. M, molecular weight standard.

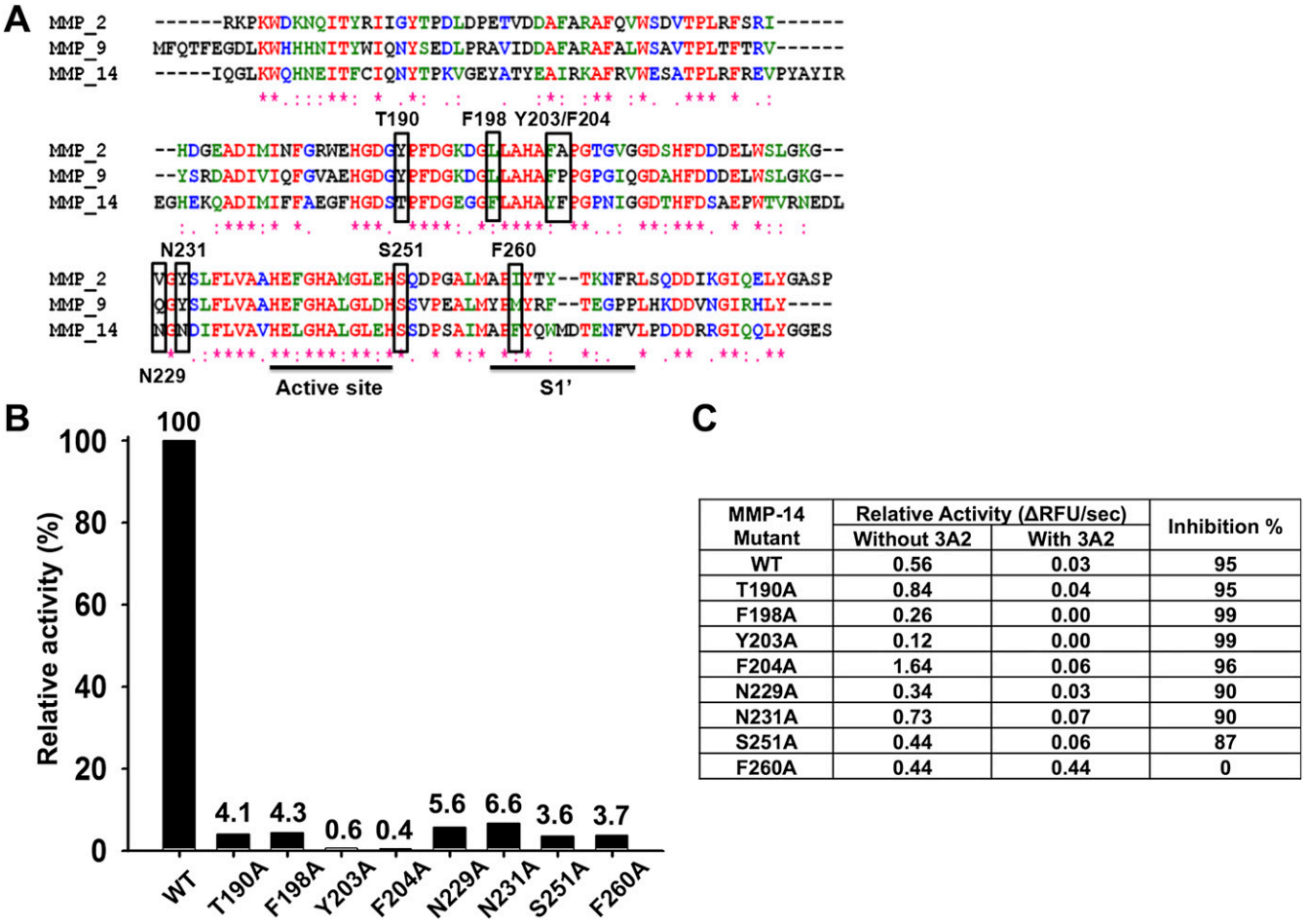

MMP-14 Mutant	Relative Activity (ΔRFU/sec)		Inhibition %
	Without 3A2	With 3A2	
WT	0.56	0.03	95
T190A	0.84	0.04	95
F198A	0.26	0.00	99
Y203A	0.12	0.00	99
F204A	1.64	0.06	96
N229A	0.34	0.03	90
N231A	0.73	0.07	90
S251A	0.44	0.06	87
F260A	0.44	0.44	0

Fig. S8. MMP-14 mutants for epitope mapping. (*A*) Sequence alignment of catalytic domains of human MMP-2, MMP-9, and MMP-14. The active site (HEXXHXXGXXH) and the S1′ region are underlined. The mutation sites chosen for epitope mapping are boxed. Identity residues are shown in red and marked with an asterisk. The residues of strong similarity are shown in green and marked with a colon. The residues of weakly similarity are shown in blue and marked with a period. The residues of nonidentity are shown in black. Sequence identity in these three MMPs is 37.43%. Sequence similarity in these three MMPs is 29.05%. (*B*) Activity of each mutant (10 nM) was monitored in the presence of 1 μM quenched fluorescent substrate. The slope of each mutant was measured, and the relative activity was calculated using wild-type (WT) MMP-14 as 100%. (*C*) Inhibition assay was performed using 50 nM MMP-14 mutant, 5 μM Fab 3A2, and 1 μM quenched fluorescent substrate. The inhibition percentage was derived from the relative activities of MMP-14 in the presence and absence of Fab 3A2. RFU, relative fluorescent units.

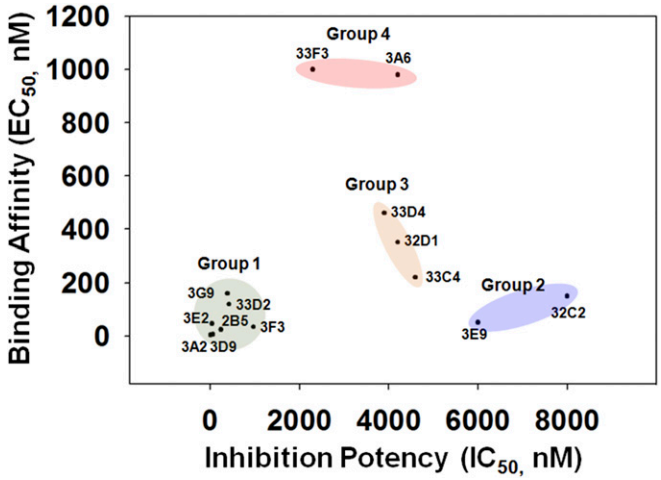

Fig. S9. Relationship between binding affinity and inhibition potency. The 14 inhibitory clones isolated in this study form four clusters: group 1 (seven of 14 clones), high inhibition potency and high binding affinity; group 2 (two of 14 clones), high binding affinity and low inhibition potency; group 3 (three of 14 clones), moderate binding affinity and moderate inhibition potency; and group 4 (two of 14 clones), low binding affinity and moderate inhibition potency. Clones in group 1 can serve as leads for further characterizations. Clones in group 2 presumably have their paratopes partially contribute to inhibition. Clones in groups 3 and 4 probably bind to inhibitory epitopes with suboptimal strengths and are therefore suitable for further affinity maturation.